P2.20 SEASONAL HEAT BUDGET OF THE CALIFORNIA CURRENT

Kathleen A. Edwards and Kathryn A. Kelly*
University of Washington, Seattle, Washington

1. INTRODUCTION

The California Current is a biologically important site of strong air-sea exchanges of momentum, moisture, and heat. We investigate the latter through an upper-ocean heat budget along a San Francisco-Honolulu section (Fig. 1), where volunteer observing ships have dropped temperature probes (XBTs) for several decades. Since September 1991, the resolution of the XBT data collected along this line has increased with WOCE support (Roemmich et al., 2001). The XBT data have been used by many researchers to estimate oceanic heat content (e. g. Emery, 1976), as we do here.

2. METHODS

We estimate an oceanic heat budget for this vertical section from the temperature tendency equation,

$$\frac{\partial T}{\partial t}+\underset{\sim}{v}\cdot\nabla T+w\frac{\partial T}{\partial z}=\frac{1}{\rho c_p}\frac{\partial q}{\partial z} \qquad (1.1)$$

Integrating (1.1) vertically to a depth *h* gives

$$\frac{\partial H}{\partial t}+\int_h^0 \underset{\sim}{v}\cdot\nabla T dz+\int_h^0 w\frac{\partial T}{\partial z}dz=\frac{1}{\rho c_p}\int_h^0\frac{\partial q}{\partial z}dz \qquad (1.2)$$

where *H* is the vertically averaged heat content from the XBT profiles. Integrating (1.2) in time gives and equation for the heat content,

$$H=-\int\int_h^0 \underset{\sim}{v}\cdot\nabla T dzdt+\frac{1}{\rho c_p}\int Q_0 dt \qquad (1.3)$$

where we have chosen to integrate to a sufficient depth that the contribution of vertical motions (Emery, 1976) and vertical heat fluxes at that depth are assumed to be negligible. Heat content integrated down to 500 m had the same gross features as either integrating down to 800 m or to an isotherm defining the top of the permanent thermocline, but with less noise, and so is presented here. The net surface heat flux $Q_0=Q^{LH}{}_0+Q^{SH}{}_0+Q^{SW}{}_0+Q^{LW}{}_0$ is the sum of the latent, sensible, shortwave, and longwave heat fluxes.

Our goal is to estimate the right-hand terms of (1.3) from globally available satellite data, creating a budget that could be constructed along other long-term XBT tracks. Each term in (1.3) is interpolated onto the ship track (Fig. 1), and a seasonal cycle is computed by fitting a cosine representing the first and second annual harmonic to its time series (Lynn, 1967). It will be presented with the annual mean removed. When present, the second harmonic can shift, broaden, or sharpen the annual peak. The seasonal cycle allows datasets of different time coverage to be combined, such as the TOPEX/POSEIDON altimeter (1999-present) and ISCCP surface radiation budget (1983-2001). Where the fit explains less than 4% of the variance, the seasonal cycle is discarded.

As is shown by (1.3), the oceanic heat content is an integrator of atmospheric forcing and so can be used to validate atmospheric flux products. Recently, several global estimates of daily turbulent heat flux components have been made by applying bulk flux algorithms to satellite-derived surface fields. Table 1 lists four such products: HOAPS (Hamburg Ocean Atmosphere Parameters and Fluxes from Satellite Data), J-OFURO (Japanese Ocean Flux data sets with Use of Remote sensing Observations), GSSTF-2 (Goddard Satellite-Based Surface Turbulent Fluxes), and a CERSAT (Centre ERS d'Archivage et de Traitement) product. As well, surface radiative fluxes have been estimated by applying radiative transfer models to top-of-the-atmosphere radiation observations such as those collected during ISCCP (International Satellite Cloud Climatology Project). These products compete with operational products like NCEP for uses such as forcing oceanic models. One goal of the current project is to compare how these flux products perform in the California Current region, based on the seasonal heat budget in (1.3).

Heat advection is attributed to Ekman and geostrophic transport. The former is,

$$\int_h^0 \underset{\sim}{v}_E\bullet\nabla T dz\sim\left(\frac{\tau}{\rho f}\times\hat{k}\right)\bullet\nabla T_0 \qquad (1.4)$$

where the wind stress, τ, is estimated from gridded QuikSCAT data, and it is assumed that the Ekman layer temperature can be approximated by the sea surface temperature, T_0, from TRMM, while the return flow at depth is assumed to transport negligible heat. The depth-integrated geostrophic transport is assumed to be proportional to surface values,

$$\int_h^0 \underset{\sim}{v}_g\cdot\nabla T dz\propto h\left(\frac{g}{f}\hat{k}\times\eta\right)\bullet\nabla T_0 \qquad (1.5)$$

where *g* is the gravitational constant, *f* is the Coriolis parameter, and η is the sum of the sea surface height anomaly from TOPEX/POSEIDON and a mean sea surface height from regional drifter data (Kelly et al., 1998). A 0.5 constant of proportion is used, based on vertical profiles of geostrophic heat transport calculated from SODA model fields (Carton et al., 2000).

* *Corresponding author address:* Kathleen A. Edwards, Applied Physics Laboratory, Univ. of Washington, Seattle, WA 98105-6698; e-mail: edwards@apl.washington.edu.

3. RESULTS

3. a. Heat budget

The seasonal cycle of the heat budget terms is shown in Figures 2-5. The heat content (Figure 2) resembles the net heat flux (Figure 3) offshore, as was found in Moisan and Niiler (1998). Inshore of ~500 km, however, the phase of the heat content shifts so that its maximum occurs earlier in the year, while the phase of the net heat flux does not change. The crossshore phase shift is the signature of the advective terms, which are dominated by the geostrophic transport of the California Current (Figure 4). When the heat flux and transport are added (Figure 5), the sum qualitatively resembles the heat content in magnitude and phase, as well as the heat content estimated from altimetric SSH (not show). Defining the California Current as containing equatorwards velocities exceeding 3 cm/s gives an annual mean width of the Current of ~440 km, increasing over the summer to a ~530 km seasonal maximum in early October.

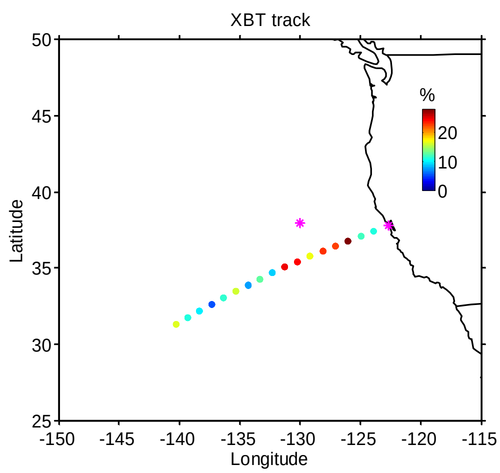

Figure 1: Heat budget is estimated at locations shown. Color indicates % of variance explained by the seasonal cycle. Locations of NDBC buoys are starred. Alongshore (crossshore) transports is across (along) the track.

	LH	*SH*	*LW*	*SW*	*Source*	*Reference*
GSSTF-2	X	X			SSM/I, NCEP	Chou et al. (1997)
HOAPS	X	X	X		SSM/I, AVHRR	Schlussel et al. (1995)
J-OFURO	X	X	X		SSM/I, Reynolds SST, ECMWF	Kubota et al. (2002)
CERSAT	X				SSM/I, ERS, AVHRR	Bentamy et al. (2003)
ISCCP			X	X	GOES	Gupta et al. (1999)
NCEP	X	X	X	X	Model	Kanamitsu et al. (2002)
COADS	X	X	X	X	Ship observations	Josey et al. (1998)
Buoy	X	X			NDBC	COARE algorithm (Fairall et al., 2003)

Table 1: Flux products used in the analysis. The first 5 are based on satellite data.

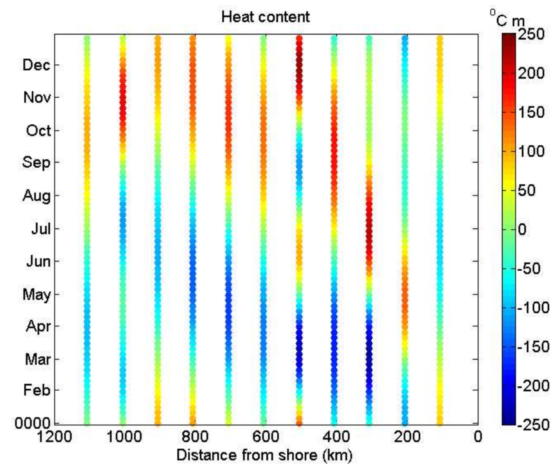

Figure 2: For alongtrack locations of Figure 1, seasonal cycle fit to heat content. Annual mean is removed from this and all other plots.

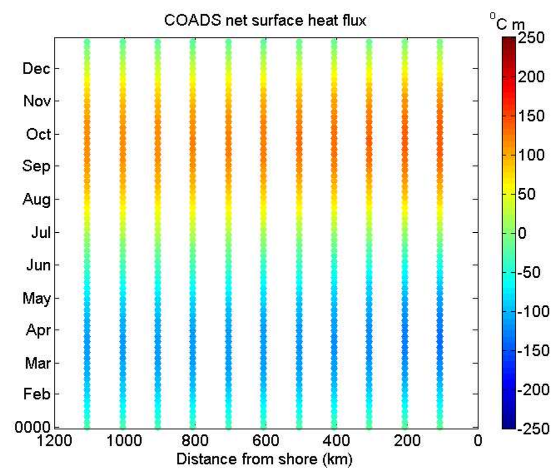

Figure 3: COADS net surface heat flux (Josey et al., 1998) contribution to heat budget. The time-integrated forcing terms will be presented in all plots.

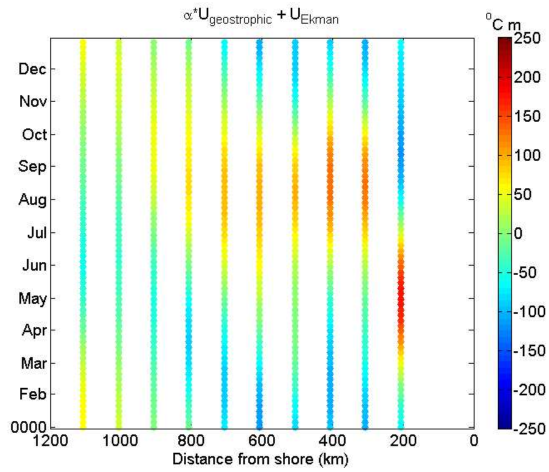

Figure 4: Heat transport.

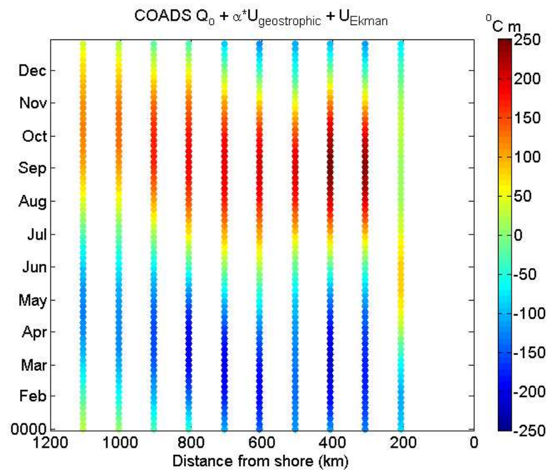

Figure 5: Sum of transport and net heat flux terms, which should match the heat content (Figure 2).

3. b. Heat flux product comparison

The heat budget can use it to test the heat flux products listed in Table 1. Fall is the time of greatest seasonal heat flux and due to the dominance of the annual cycle, the minimum in spring is its mirror image (Fig. 3). Therefore, the seasonal cycle at mid-fall is shown in Figs. 6 and 7. In Fig. 6, the latent, sensible, and longwave heat flux components are compared along the ship track. The solid line is the COADS ship-based climatology, while the filled symbols are from nearby buoys (Fig. 1). The latent heat flux contribution is the greatest of the three, with lesser magnitude towards the coast. The crossshore change in sign evidenced by HOAPS and J-OFURO is supported by the buoy at 600 km offshore, and these products magnitude offshore resembles the COADS product, which however does not change sign nearshore. The HOAPS longwave flux has greater magnitude than COADS. However, Fig. 7 shows that the ISCCP longwave heat flux also has greater magnitude than COADS. Because it ingests NCEP variables, the GSSTF-2 fluxes strongly resemble NCEP. The two have the largest latent heat flux magnitude and lack a discernable seasonal cycle near the coast.

In Fig. 7, all terms of the heat budget are compared for COADS, ISSCP, and NCEP. The shortwave heat flux dominates. The magnitude of the shortwave heat flux from NCEP exceeds that from both ISSCP and COADS by ~25^{o}Cm. The NCEP Reanalysis-2 used in this comparison underpredicts stratus clouds characteristic of the California Current region, increasing the amount of shortwave radiation reaching the sea surface and thus the shortwave flux. A ~25% increase in the net heat flux is produced relative to the other products, which is approximately the magnitude of the other flux component; a similar increase is seen in the annual mean (not shown). After the shortwave heat flux, the latent heat flux makes the next largest contribution, followed by the longwave and nearly negligible sensible heat flux components. The seasonal cycle of the latent heat flux products differ by phase (not shown) as well as magnitude, with the greatest divergence within ~500 km from shore.

The predictive skill of the Table 1 flux products within the California Current seasonal heat budget (Figs. 8-9) is defined to be the fraction of heat content variance that each explains, when added to the other flux components from COADS to make up the net surface heat flux. Perfect skill has a value of 1, no skill has a value of 0, and negative values occur when the prediction is worsened by including the predictor. A key feature is the similarity between the products' skill, which seldom differs by more than 0.25. In the case of longwave and sensible flux, the products' skills (not shown) are nearly indistinguishable, due to their small contribution to the budget. Due to the greater role of advection nearer shore, all flux-only products (i.e. without inclusion of advection) lose skill close to the coast. The greatest skill comes from the shortwave heat flux (Fig. 8), with similar performance from the NCEP, ISCCP, and COADS products except near shore, where all have negative skill and NCEP has the least. Near-unity values imply that the shortwave heat flux alone provides a fair representation of the seasonal heat content offshore. For latent heat flux (Fig. 9), the products' skills are close, with a slight lead by CERSAT.

To consider the ability of the advective terms to improve the heat budget's skill near the coast, Fig. 9 compares the skill of the COADS net heat flux with and without the addition of advection. Offshore, the inclusion of heat transport reduces the skill, which we attribute to the imperfection of our advection estimate, but within ~500 km of the coast, the skill is either unchanged or, adjacent to the coast, significantly improved. This highlights the role of the eastern boundary current in transporting heat gained by the ocean from the atmosphere.

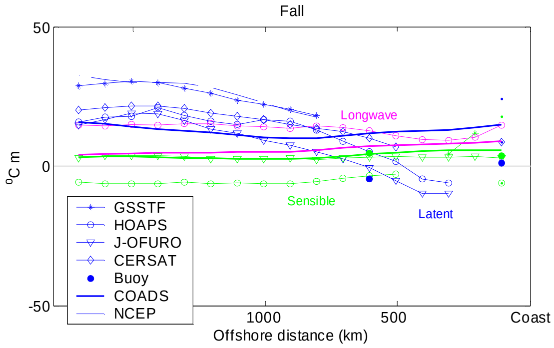

Figure 6: Latent, sensible, and longwave heat flux for fall, a maximum in the seasonal cycle.

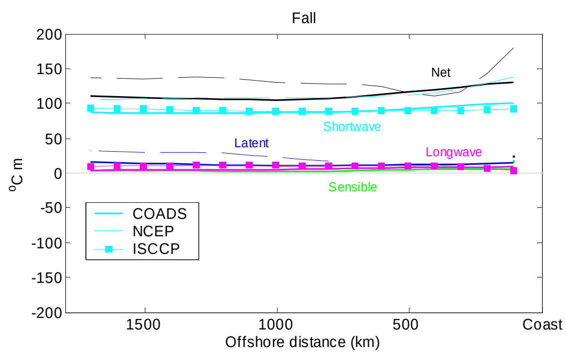

Figure 7: All heat flux terms for fall.

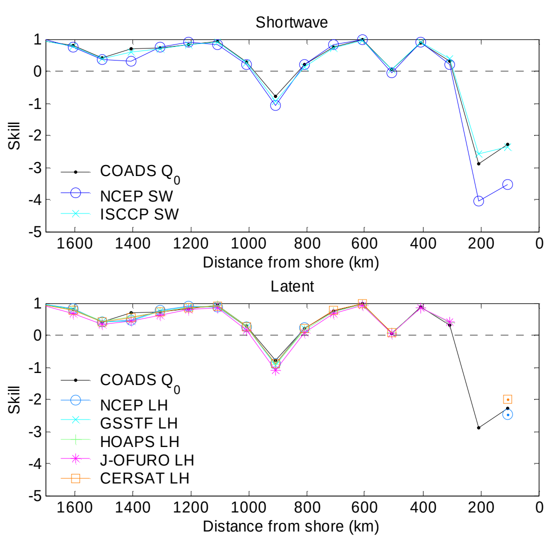

Figure 8: For the flux products in Table 1, heat content skill of (top) shortwave and (bottom) latent heat flux components when substituted into COADS net flux.

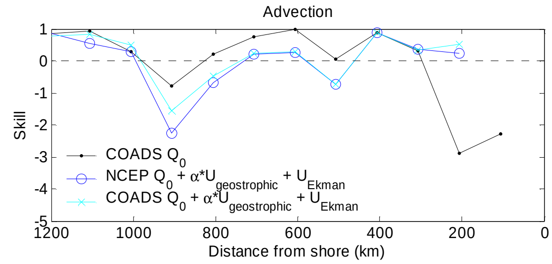

Figure 9: Skill for COADS net heat flux; COADS plus heat transport; NCEP plus heat transport.

4. REFERENCES

Bentamy, A., K. B. Katsaros, A. M. Mestas-Nuñez, W. M. Drennan, E. B. Forde, and H. Roquet, 2003: Satellite estimates of wind speed and latent heat flux over the global oceans. *J. Climate,* **16**, 637–656.

Carton, J. A., G. Chepurin, X. Cao, B. Giese, 2000: A Simple Ocean Data Assimilation Analysis of the Global Upper Ocean 1950–95. Part I: Methodology. *J. Phys.Ocean*. **30**, 294–309.

Emery, W., 1976: The role of vertical motion in the heat budget of the upper northeaster Pacific Ocean. *J. Phys. Oc*., **6**, 299-305.

Fairall, C. W., Bradley, E. F., Hare, J. E., Grachev, A. A., Edson, J. B.. 2003: Bulk Parameterization of Air–Sea Fluxes: Updates and Verification for the COARE Algorithm. *J. Clim,* **16**, 571–591.

Gupta, S. K., N. A. Ritchey, A. C. Wilber, C. H. Whitlock, G. G. Gibson, and P. W. Stackhouse, 1999: A climatology of surface radiation budget derived from satellite data*. J. Clim.* **12**., 2691-2710

Chou, S.-H, C. -L. Shie, R. M. Atlas, and J. Ardizzone, 1997: Air-sea fluxes retrieved from special sensor microwave Imager data*. J. Geophys. Res.*, **102**, 12705-12726.

Josey, S. A., E. C. Kent and P. K. Taylor, 1998: The Southampton Oceanography Centre (SOC) Ocean - Atmosphere Heat, Momentum and Freshwater Flux Atlas. *Southampton Oceanography Centre Report***,** **6**, 30 pp. plus figs.

Kanamitsu, M. W. Ebisuzaki, J. Woollen, S-K Yang, J.J. Hnilo, M. Fiorino, and G. L. Potter, 2002: NCEP-DEO AMIP-II Reanalysis (R-2). *Bull. Amer. Met. Soc.,* **83**, 1631-1643.

Kelly, K.A., R. C. Beardsley, R. Limeburner, K. H. Brink, J. D. Paduan, and T.K. Chereskin, 1998: Variability of the near-surface eddy kinetic energy in the California Current based on altimeter, drifter, and moored current data, *J. Geophys. Res,* **103**, 13,067-13,083*.*

Kubota M.., K. Ichikawa, N. Iwasaka, S. Kizu, M. Konda and K. Kutsuwada, 2002: Japanese Ocean Flux Data Sets with Use of Remote Sensing Observations (J-OFURO), *J. Oceanog*., **58**, 213-225.

Lynn, R. J. 1967: Seasonal variation of temperature and salinity at 10 m in the California Current. *Calif. Coop. Oceanic Fish. Invest. Rep.*, **19**, 157-174.

Moisan, J. and P. Niiler, 1998: The seasonal heat budget of the North Pacific: Net heat flux and heat storage rates (1950-1990). *J. Phys. Oc.,* **28**, 401-421.

Roemmich, D., J. Gilson, B. Corneulle, and R. Weller, 2001: Mean and time-varying meridional transport of heat at the tropical/subtropical boundary of the North Pacific Ocean. *J. Geophys. Res.,* **106**, 8957-8970.

Schlussel, P., L. Schanz, and G. Englisch, 1995: Retrieval of latent heat flux and longwave irradiance at the sea surface from SSM/I and AVHRR measurements. *Adv. Space Res.,* **16**, 107-116.